

Three-dimensional skyrmionic cocoons in magnetic multilayers

Matthieu Grelier¹, Florian Godel¹, Aymeric Vecchiola¹, Sophie Collin¹, Karim Bouzehouane¹, Albert Fert¹, Vincent Cros¹, Nicolas Reyren¹

¹ *Unité Mixte de Physique, CNRS, Thales, Université Paris-Saclay, 91767, Palaiseau, France.*

Abstract

Three-dimensional (3D) topological spin textures emerge as promising quasi-particles for encoding information in future spintronic devices. The third dimension provides more malleability regarding their magnetic properties as well as more flexibility for potential applications. However, the stabilization and characterization of such quasi-particles in easily implementable systems remain a work in progress. Here we observe a new type of 3D magnetic textures that we called skyrmionic cocoons that sits in the interior of magnetic thin films multilayers and possesses a characteristic ellipsoidal shape. Interestingly, these cocoons can coexist with more standard ‘tubular’ skyrmions going through all the multilayer as evidenced by the existence of two very different contrasts in the MFM images recorded at room temperature. The presence of these novel skyrmionic textures as well as the understanding of their layer resolved chiral and topological properties have been investigated by micromagnetic simulations. In order to experimentally stabilize the combination of 3D skyrmion tubes and cocoons, we have elaborated metallic multilayers in which the magnetic properties, notably the anisotropy, of the magnetic films in the stacks is varied depending on their vertical position. Finally, in complement to the magnetic imaging, we also measure the magneto-resistive response of the multilayers as a function of the magnetic field, and succeed to fit its evolution using the 3D micromagnetic simulations as inputs for the magnetic configuration. The excellent agreement that is reached brings additional evidence of the presence of skyrmionic cocoons that hence can be electrically detected.

Introduction

Topological magnetic textures have been under close scrutiny in recent years as they could represent an original asset for the development of new logic and memory devices as well as novel hardware neuromorphic nanocomponents [1]. Chiral magnets and magnetic multilayers allow for the stabilization of two-dimensional (2D) textures that have been extensively investigated [2]. A key example remains the magnetic skyrmion, [3] a 2D whirling of the magnetization which is therefore uniform along the vertical dimension (the dimension normal to the film), first observed in B20 chiral magnets [4]. In thicker structures, skyrmion tubes can also be stabilized, thus adding a vertical dimension that presents small variations depending on the equilibrium of the magnetic interactions at play [5]. More recently however, interest has surged for three-dimensional (3D) nanomagnetism and consequently for complex textures displaying an important evolution over the thickness [6], [7], leading to the discovery of new categories of topological textures. For instance, in bulk material, theoretical predictions, followed by experimental observation, describe magnetic bobbars [8], [9] where one end of a skyrmion string goes to a surface while the other one ends with a point singularity inside the

sample. Another case of these skyrmions strings corresponds to dipole string [10], so named due to the two Bloch points at their extremities. Analogous textures have been reported as well in magnetic multilayers with the recent observation of the elusive hopfion [11], [12], originally predicted to appear in chiral magnetic crystals [13], [14]. It was also shown that, in hybrid ferromagnetic/ferrimagnetic multilayers, truncated skyrmions that ends abruptly at a given interface can be stabilized [15], [16]. Such new objects pave the way toward expending spintronics into the third dimension but several challenges must be overcome first, mostly their characterization as well as their implementation. Regarding the former, studying such textures require to probe the magnetization over the thickness which is often achieved by using recent high-end imaging techniques that rely on the use of soft X-rays or electrons. For example, remarkable reconstructions have been achieved for a permalloy disk using x-ray laminography [17] or for various textures with x-ray tomography [18], [19], [20], [21]. As a less challenging and restrictive alternative, we will put forward a simpler approach based on magneto-transport measurements that can be accurately coupled with micromagnetic simulations not only to detect 3D objects but to resolve their magnetization profile as well. Concerning their implementation, most of those newly observed textures have been detected in chiral magnetic crystals or in nano-structures which strongly limits their functionality. In opposition, multilayers appear as a promising alternative to harbor 3D topological textures as they are more resilient and scalable while offering a broader tunability of their magnetic properties. Indeed, tuning the films thickness and the interfaces properties helps to control various magnetic interactions, notably the Dzyaloshinskii-Moriya interaction (DMI) [22], [23], [24], an asymmetric exchange facilitating the stabilization of topological non-collinear textures [25], [26]. Based on this strong malleability, we have developed original multilayers architectures that allows the stabilization of a new type of 3D spin texture, the skyrmionic cocoon, which could ultimately serve as a basis for 3D skyrmionic devices.

Engineering of the multilayer properties

In order to induce the stabilization of 3D magnetic textures, we exploit the tunability of the magnetic multilayers by engineering an elaborated sample architecture (Fig. 1a) with a variable thickness for the ferromagnetic material to introduce an uneven distribution of the magnetic interactions over the vertical dimension. Typically, the multilayers are made of repetitions of the trilayers Pt 3 nm/Co X_i /Al 1.4 nm, with X_i the Co thickness of the i^{th} magnetic layer. This trilayer system has been chosen as we recently showed that it maximizes the interfacial DMI [23], which usually facilitate the stabilization of chiral spin textures. This first sample heterostructure, that we call single gradient (SG), is designed with a specific evolution for the ferromagnetic thickness: it transitions from the initial value X_1 to X_{max} with a fixed thickness step and then come back to the initial thickness, following the same steps in reverse order. In other words, the Co thickness X_i can be recursively defined as:

$$X_{i+1} = \begin{cases} X_i + S & \text{for } i \leq N/2 \\ X_i - S & \text{for } i > N/2 \end{cases}, \quad (1)$$

with S the thickness step between two consecutive layers, N the total number of layers and X_1 the bottom layer thickness. A scheme of the multilayer is drawn in Fig. 1a, showing the thickness evolution as a function of the layer index i where the outer layers are the thinnest ones ($S > 0$). By tuning S and the external perpendicular magnetic field, the vertical confinement of the magnetic textures can be controlled (Suppl. Mater. Section 1 and Fig. S1). In the following, we focus on the structure parameters used in Fig. 1, namely $X_1 = 1.7$ nm, $S = 0.1$ nm and $N = 13$ layers, that correspond to the sample which has been experimentally

characterized and studied in detail with micromagnetic simulations (see Method for detailed structure). Since the reorientation transition thickness was measured to be 1.7 nm in our Pt/Co/Al trilayers, the multilayer under consideration should mostly display an in-plane (IP) effective anisotropy (see Fig. S2 for magnetization curves).

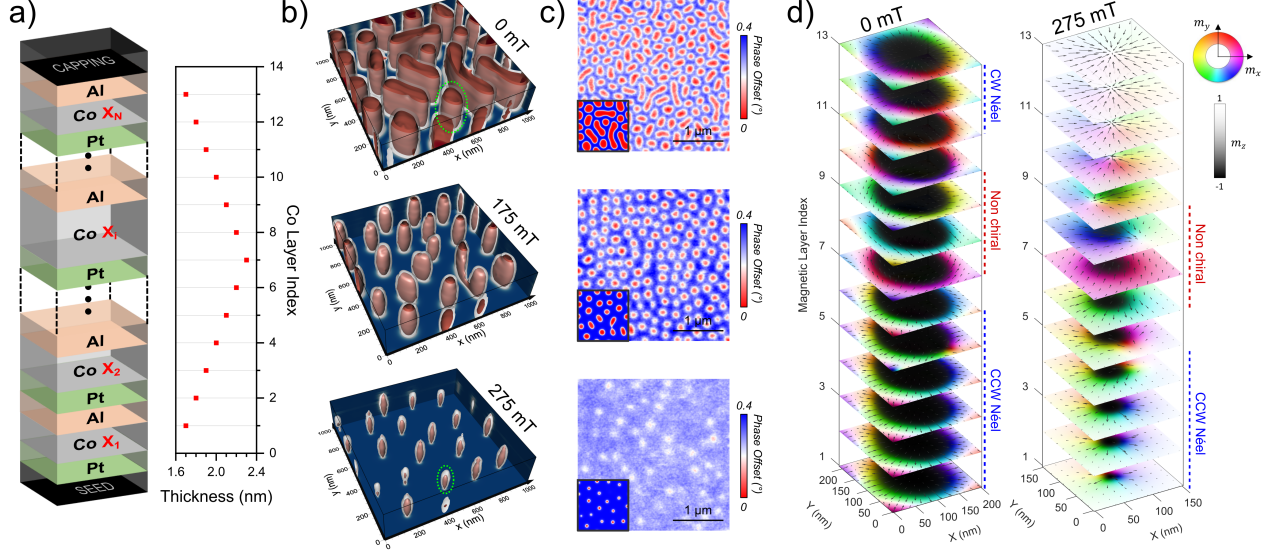


Figure 1: Properties of Single Gradient (SG) multilayers with parameters $S = 0.1$ nm, $X_1 = 1.7$ nm, $N = 13$ layers. a) Scheme of a typical SG multilayer, defined by the number of layers N , the thickness step S , and the starting thickness X_1 . The lateral plot shows the Co thickness evolution. b) Field evolution of the magnetic textures with micromagnetic simulations after an out-of-plane saturation displayed with isosurfaces (in red, $m_z = -0.8$, in white, $m_z = 0$ and in dark blue, $m_z = 1$). c) Corresponding phase map images obtained with MFM accompanied by simulated ones ($1 \times 1 \mu\text{m}^2$) at the bottom left corner. The experimental magnetic fields correspond to the simulated ones ± 10 mT and point out-of-plane. d) Magnetization cuts of a selected object, indicated in b) by the green dotted ellipses, at two different magnetic fields to evidence the vertical evolution and the chirality (CW: clockwise, CCW: counterclockwise).

In order to apprehend the actual shape and magnetization distribution of the objects hosted in SG structures, we perform micromagnetic simulations using *Mumax3* [27]. To help the visualization of the 3D objects, their output is displayed making use of the isosurfaces $m_z = -0.8$ in red, $m_z = 0$ in white and $m_z = 1$ in dark blue (only shown in the background planes). In Fig. 1b, the relaxed states after an out-of-plane (OOP) initialization are shown for three different OOP magnetic fields. At zero field, considering a planar cut, an irregular lattice of circular objects and more elongated ones is found. Both kinds are columnar, *i.e.* they are extending from the bottom to the top interface. Increasing H_\perp up to 175 mT reduces their size and homogenizes their shape due to the Zeeman effect gaining in strength, resulting in a configuration more similar to a lattice of skyrmion tubes. Then at 275 mT, they become vertically confined and remain in a fraction of the layers only, acquiring a characteristic deformed ellipsoid shape. Based on this vertical confinement and their peculiar profile, we name them skyrmionic cocoons.

To experimentally characterize those new 3D magnetic textures, we first use magnetic force microscopy (MFM) measurements. In Fig. 1c, experimental phase maps are shown alongside with the simulated MFM images in the inserts obtained from the previously described micromagnetic simulations. The agreement

between the simulations at the three chosen fields and the actual magnetic configuration is satisfying: at zero field, a distribution of inhomogeneous skyrmionic tubes is measured that then acquire a barrel shape in the vertical direction as $\mu_0 H_\perp$ reaches 175 mT. Then for even higher fields *e.g.* 275 mT, in such SG, we clearly observe a decrease in MFM phase contrast coming from the fact that the detected objects are more and more buried under the top surface. This behavior is in qualitative agreement with the corresponding micromagnetic simulations which thus appear to appropriately model the density, the shape and the size of the observed objects.

In Fig. 1d, we present layer-resolved magnetization profiles simulated at 0 and 275 mT. These profiles clearly evidence the evolution from a fully columnar skyrmion to a vertically confined skyrmionic cocoon. Moreover, these simulations allow to discriminate the effective chirality of the spin textures in each magnetic layers composing the multilayers. For the case of skyrmion tubes at zero field, we find that the bottom layers (1 to 6) are counterclockwise (CCW) Néel type whereas in their top layers (11 to 13) they are clockwise (CW) Néel. This distribution is expected as the CCW chirality is favored by the equilibrium between the interfacial DMI for the chosen stacking sequence and the dipolar field. In the remaining middle layers, the skyrmion walls display a magnetization pointing uniformly in the same in-plane direction as the interlayer dipolar interaction and the DMI nearly cancel each other out. The resulting local textures change significantly for $\mu_0 H_\perp = 275$ mT: the skyrmion tube evolves into a cocoon as the core shrinks and then disappear in the outer layers. Indeed, in the top part (layers 9 to 13), we only observe a texture resembling a radial vortex with a minute core having the same polarity as the background, induced by the dipolar field. Note the absence of Bloch points at the extremities of the cocoons that differentiate them from similarly shaped textures like the aforementioned dipole strings. The exact topological properties of such objects are beyond the scope of this paper. Nevertheless, more detailed information about their properties are presented in the Supplementary Material (Section 5).

Coexistence of skyrmionic cocoons and tubes

Based on the properties of skyrmionic cocoons identified in SG multilayer, we decide to push further the engineering and the complexity of the multilayers to investigate how these new 3D magnetic objects can be combined with other textures. Beyond the fundamental interest, for example to study the transition processes between topologically different magnetic textures, the purpose here is also to investigate how these cocoons can be intentionally localized at different z-positions, that in the perspective of applications, would be a first step in the design of 3D skyrmionic platforms. The chosen multilayer structure presented in Fig. 2a is called Double Gradient (DG), as it includes 2 SG blocks separated by a number M of trilayers with thin Co of constant thickness Y that thus have a strong perpendicular magnetic anisotropy (PMA). In the following, we focus on the architecture defined by $X_1 = 2.0$ nm, $S = 0.1$ nm, $Y = 1.0$ nm, $N = 13$ layers and $M = 15$ repetitions.

In Fig. 2b, we present the MFM images recorded at remanence after different initialization processes and the corresponding simulated MFM images. First, saturating the sample magnetization in-plane (IP) results in stripes with various branching giving a single MFM contrast. This indicates that the textures are columnar and thus go through all the layers, as confirmed by the 3D micromagnetic simulations (not shown). In case of an initialization with an OOP field, two different contrasts are clearly visible (white and grey) in the MFM. The related simulations told us that such a case is representative of the presence of two different objects. Note the size of the smallest features that can reach sub-100 nm size at zero field. Finally, the case of

a tilted field during the initialization leads to a configuration containing distorted stripes with dots of lower contrasts in their midst.

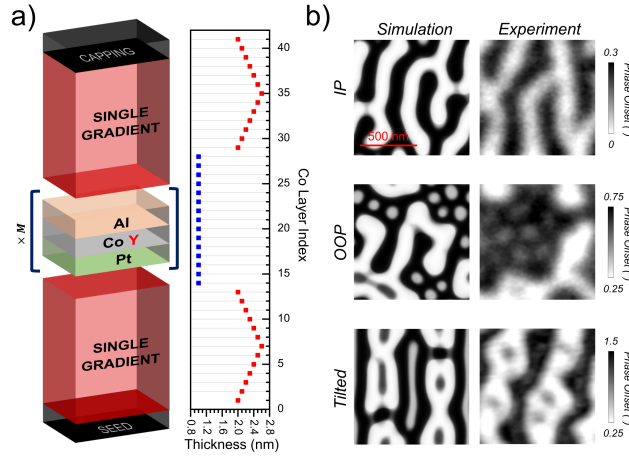


Figure 2: Remanent magnetic configuration in DG multilayer with parameters $X_1 = 2.0$ nm, $S = 0.1$ nm, $Y = 1.0$ nm, $N = 13$ layers, $M = 15$ repetitions. a) Schematic structure with additional parameters of the thin Co thickness Y and the associated number of repetitions M . The lateral plot shows the Co thickness evolution. b) Simulated and experimental phase maps for different magnetic history. For the simulations (resp. the measurements), the sample was either saturated (resp. demagnetized) OOP, IP or with a tilted magnetic field, 30° away from the normal (resp. 60°). All images share the same length scale, displayed in the top left image.

In Fig. 3a we present the MFM images corresponding to the tilted field evolution. As shown before, at $\mu_0 H = 0$ mT, we can distinguish two kinds of textures: first the ones that penetrate through all the layers, *i.e.*, the columnar stripes, and second the skyrmionic cocoons. For simplicity, we will refer to the former as 3D stripes (or worms) in the following. The strong contrasts therefore corresponds to the columnar objects whereas the cocoons are associated with a weaker signal. The corresponding micromagnetic simulations (see Fig. 3b) indicates that in most cases, two cocoons are present, one in each SG block, and that they sits one on top of the other. For a larger OOP magnetic field (230 mT), the red 3D stripes become narrower and the density of cocoons increases, yielding a configuration showing alternatively stripe domains and chain of cocoons. For a slightly higher field, at 350 mT (resp. 275 mT) in the simulations (resp. experiments), the elongated side of the 3D stripes shrinks, causing them to transition into skyrmion tubes (large red dots) whereas the cocoons (white small dots) appear more resilient to the field. Finally, when the field is high enough, at 400 mT, the layers with strong PMA point uniformly in its direction, thus transforming the remaining skyrmion tubes into two cocoons, one in each gradient. We hence identify a field range in which we can stabilize cocoons in separated blocks which could be piled up in more complex architectures. The exact nature of the transitions at play and their associated mechanisms remain to be elucidated. Finally, note that in the simulations, most of the cocoons appear to be vertically aligned with another. As the MFM signal comes mainly from the stray field of the top layers, this cannot be yet confirmed experimentally. To do so, more advanced 3D imaging techniques such as laminography would be necessary in order to resolve the precise distribution of the magnetization.

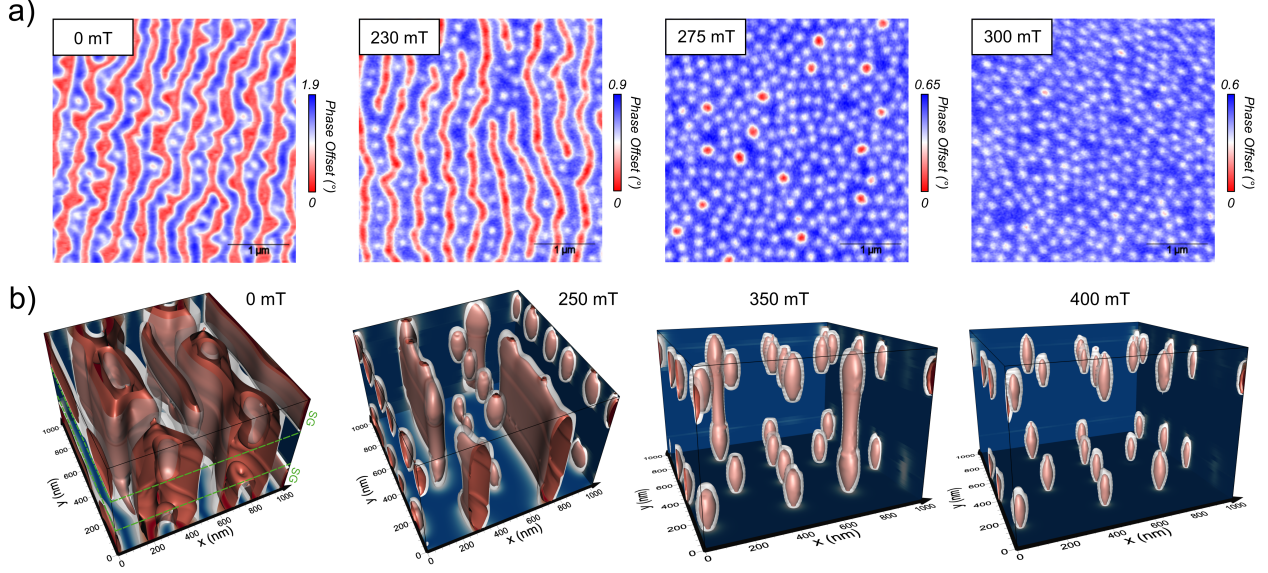


Figure 3: DG multilayer field dependency. a) Experimental MFM phase maps measured after a 30° demagnetization (away from the normal). b) Relaxed states of micromagnetic simulations, displayed with isosurfaces (in red, $m_z = -0.8$, in white, $m_z = 0$ and in dark blue, $m_z = 1$), at various magnetic field starting from a 60° initialization. The magnetic field is applied perpendicularly to the sample.

Measuring the electrical signature of cocoons

To investigate the presence of cocoons in the bottom layers, in addition to the MFM imaging, we perform magneto-transport measurements in Hall bar devices of size $20 \times 100 \mu\text{m}^2$ in the previously studied DG multilayer to probe their electrical properties. We measure both the longitudinal resistance R_{xx} and the transverse resistance R_{xy} while sweeping the magnetic field along different orientations. In order to fit these electrical measurements, a simple model taking into considerations several possible contributions to the magneto-resistive effects is considered [28]. The current is injected along x , the film normal is along z and θ corresponds to the angle between z and the field (see inset of Fig. 4a). First, due to the presence of heavy metallic layers in contact with the magnetic films, the spin Hall effect (SHE) in the heavy metal gives rise to the spin Hall magnetoresistance (SMR) [29], that depends on the angle between the magnetization \mathbf{m} of the ferromagnet and the spin polarization due to the SHE [30], [31]. The change in R_{xx} due to the corresponding SMR is thus proportional to m_y^2 . The second contribution is the anisotropic magnetoresistance (AMR) [32], that is proportional to m_x^2 , *i.e.* when the magnetization is parallel to the current. Finally, the evolution of the transverse resistance is governed by the anomalous Hall effect (AHE) [29], [33], that is proportional to the out-of-plane component of the magnetization: $R_{xy} \propto m_z$. From those considerations, R_{xx} and R_{xy} can be written as:

$$R_{xx} = R_{xx}^0 + R_{\text{SMR}} m_y^2 + R_{\text{AMR}} m_x^2, \quad (2)$$

$$R_{xy} = R_{xy}^0 + R_{\text{AHE}} m_z, \quad (3)$$

With R_{xx}^0 the longitudinal resistance for $\mathbf{m} = m_z \hat{\mathbf{z}}$ and R_{xy}^0 the resistance of the multilayer. The coefficients R_{AMR} , R_{SMR} and R_{AHE} are the proportionality coefficients of the associated effects. In the DG multilayer, the first two are found to be negative (see Method). Note that the contribution related to giant magne-

toresistance (GMR) is negligible and thus not considered. Moreover, as we found in previous work [34] that the topological Hall effect (THE) contribution in standard skyrmion multilayers was negligible compared to AHE, we do not include this contribution either. In Fig. 4, we display the measured resistance as a function of the applied field alongside the predicted evolution of $R_{xx}(H)$ using the m_x , m_y and m_z components from the micromagnetic simulations as inputs in the previous equations. Note that the coefficients of Eq. 2 and 3, R_{AMR} , R_{SMR} and R_{AHE} , are fixed by experimental measurements, and therefore, there are no fitting parameters for the curves in Fig. 4.

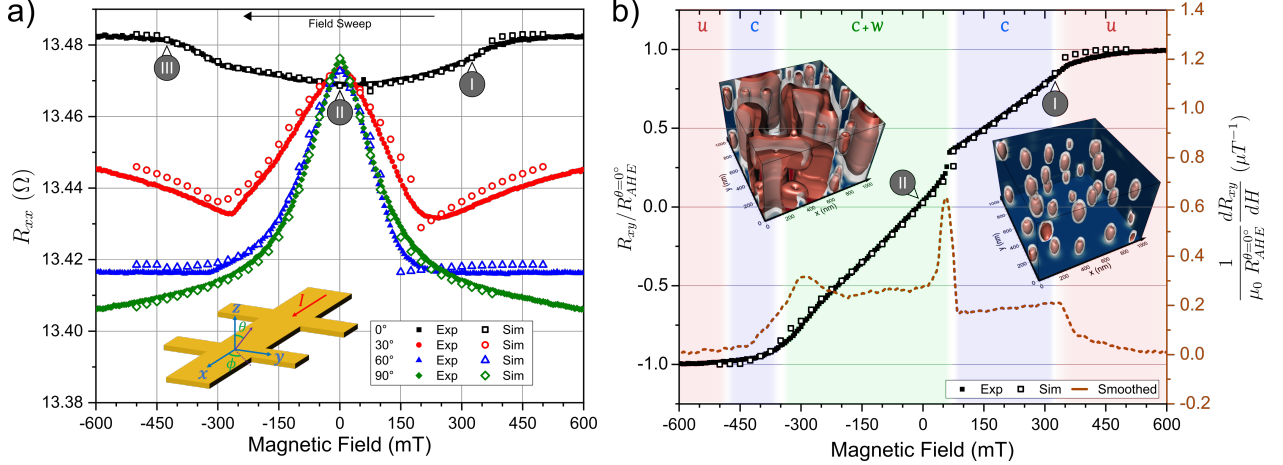


Figure 4: Electronic transport measurements on $20 \times 100 \mu\text{m}^2$ Hall bars for a DG associated with the corresponding micromagnetic simulations. a) Measurements of $R_{xx}(H)$ for different inclinations of the magnetic field. The inset shows the geometry of the experiment. b) $R_{xy}(H)$ at $\theta = 0^\circ$ (OOP field) and its derivative. The background colors corresponds to the magnetic phases (U: uniform, C: cocoons, W: worms) as predicted by the simulations. The displayed simulations are associated with the points indicated by a roman number. The experimental R_{xy} has been normalized by $R_{AHE}^{\theta=0^\circ}$ to correspond to the associated m_z value. All the displayed curves, measured or simulated, are acquired from positive field saturation, sweeping the field towards negative values in the yz plane.

In the continuity of the previous measurements, we first consider R_{xx} with an OOP field ($\theta = 0^\circ$). Only minor variations are expected since the in-plane components should remain small throughout the field sweep. Starting from high positive field to negative field, the magnetization is first saturated along the z direction until the first skyrmionic cocoons nucleate in both SG near 325 mT (state I). Their apparition create in-plane components which yield, due to the sign of the AMR and SMR, a negative contribution to R_{xx} . As they expand in all directions upon lowering $\mu_0 H$, it continues to decrease, reaching its minimum at zero field (state II). According to the simulations, it corresponds to a state in which 3D worms coexist with the skyrmionic cocoons. The symmetric trend is then observed for negative magnetic field and it is similar to the one previously described with the MFM study: the spin textures shrink and the 3D worms end up disappearing, leaving only cocoons (state III) until the sample saturates.

To further validate our approach, the field was tilted at different angles ($30, 60, 90^\circ$) in order to introduce more in-plane components. This leads to a stronger field response that challenges the sensitivity of the micromagnetic simulations. Since the magnetic field lies partially (or totally) in-plane, the nucleation events

provoke significant positive jumps in the resistance linked to a loss of IP components. It is also noticeably harder to saturate the sample along those directions due to the strong PMA layers, leaving variations at higher fields. The application of a tilted magnetic field leads to complex spin textures that are described in Suppl. Mater. (Fig. S5). At zero field however, we retrieve a state with 3D stripes and skyrmionic cocoons for $\theta = 30, 60^\circ$ whereas $\theta = 90^\circ$ yields only 3D stripes (Fig. 2). Regardless of the angle of the field, the resistances extracted from the simulations fit remarkably well the experimental ones. The difference between the two is typically of a few $\text{m}\Omega$ which can originate from the simplicity of our model and its neglected contributions as well as from some experimental angular inaccuracy (less than 0.5°).

In Fig. 4b, $R_{xy}(H)$ for $\theta = 0^\circ$ is displayed, along with its experimental derivative with a colored background associated with the different magnetic phases: uniform (red), cocoons (blue) and cocoons alongside with 3D worms (green). Based on the simulations and those curves, it is possible to identify more precisely the different magnetic phases and transitions that the sample undergoes. Near 75 mT, we can notice a jump in the resistance: it corresponds to the nucleation inside the strong PMA layers which was negligible in R_{xx} because the associated domain walls are quite narrow. Therefore, above that field, the DG multilayer host only skyrmionic cocoons in the SG blocks as illustrated with the display of state I. The field range of the associated state can be pinpointed looking at the derivative where a wide plateau is visible, before the sharp peak coming from the nucleation in the middle layers. For negative magnetic field, simulation places the regime with only cocoons between -350 and -475 mT, roughly before the small peak in the derivative near -300 mT. In the end, electrical measurements allow to recognize most of the magnetic phases of the DG multilayers and, for more precision, it can be coupled with micromagnetic simulations.

Outlook

By using variable thickness of the ferromagnetic element in magnetic multilayers, we have demonstrated the existence of skyrmionic cocoons, a new type of 3D topological magnetic texture vertically confined with sizes under 100 nm. Moreover, by studying more elaborated architectures, we have shown that they can be observed conjointly with columnar textures even in the absence of an external magnetic field and that they can be located at different vertical levels of the structure. Thanks to the excellent agreement between the simulations and the electronic transport measurements, the former give us a precise insight into the three-dimensional distribution of the magnetization as well as the different magnetic phases. This achievement also promotes magnetoresistance measurements as an easily implementable approach to detect 3D objects in such magnetic multilayers. In this study, we focused on a particular set of parameters but various other architectures based on the ones presented could be envisioned to tune the skyrmionic cocoons properties. For example, playing with the thickness step can impact their confinement and by varying the number of gradient blocks in the structure, they would have more different vertical position available. Following that reasoning, a memory device could ultimately be based on them, by encoding multiple states with the vertical position and number of cocoons for instance. Thus, this coexistence of various magnetic textures in multilayers, the discovery of those objects that we propose to call skyrmionic cocoons as well as their malleability are particularly interesting as they can open new paths for three-dimensional spintronics.

Acknowledgments

The authors are grateful to Yanis Sassi for advice on experimental techniques and simulations. Financial supports from FLAG-ERA SogrophMEM (ANR-15-GRFL-0005), from ANR under the grant ANR-17-CE24-0025 (TOPSKY) and ANR-20-CE42-0012-01(MEDYNA) and as part of the ‘Investissements d’Avenir’ program SPiCY (ANR-10-LABX-0035).

Methods

Sample preparation and characterization The samples have been grown on thermally oxidized silicon substrates using magnetron sputtering at room temperature. A seed layer of 5 nm Ta is typically used and 3 nm Pt capping is deposited to protect from oxidation. In the characterized structures, the Al is fixed at 1.4 nm whereas the Pt is 3 nm in the SG and the strong PMA part of the DG but 2 nm in the gradient parts of the DG. In details, the SG corresponds to $\text{SiO}_x||\text{Ta5}|\text{Pt3}|(\text{Co}[1.7:0.1:2.3]|\text{Al1.4}|\text{Pt3})(\text{Co}[2.2:0.1:1.7]|\text{Al1.4}|\text{Pt3})$ and the DG to $\text{SiO}_x||\text{Ta5}|\text{Pt3}|(\text{Co}[2.0:0.1:2.5]|\text{Al1.4}|\text{Pt2})(\text{Co}[2.6:0.1:2.0]|\text{Al1.4}|\text{Pt2})|(\text{Co}1.0|\text{Al1.4}|\text{Pt3})\times 15|(\text{Co}[2.0:0.1:2.5]|\text{Al1.4}|\text{Pt2})(\text{Co}[2.6:0.1:2.1]|\text{Al1.4}|\text{Pt2})(\text{Co}2.0|\text{Al1.4}|\text{Pt3})$ where the notation $[X_1 : S : X_2]$ corresponds to the thickness sequence between X_1 and X_2 with S being the thickness step. The magnetic hysteresis have been measured using AGFM (see Suppl. Mater. Fig. S2), and SQUID to determine the saturation magnetization and the corresponding paramagnetic contribution from the substrate. SQUID measurements yield a magnetization saturation of 1229 ± 18 kA/m for the SG and 1220 ± 18 kA/m for the DG.

Magnetic force microscopy and demagnetization Before imaging, the samples have been demagnetized using an electromagnet which applied an oscillating magnetic field of exponentially decreasing amplitude. The MFM images have been acquired using cantilevers from TeamNanotech (TM) with 7nm capping in a tapping mode with a lift height of 10 nm (unless mentioned otherwise), at 75 % of the drive amplitude with double-passing and at room temperature. The phase maps displayed have been modified using a Gaussian filter as implemented in Gwyddion software [35] with a 2 pixels FWHM.

Electronic transport measurements The DG sample has been patterned using UV lithography into Hall bars of dimensions $20 \times 100 \mu\text{m}^2$. Then it had been measured in a field setup with an electromagnet able to reach 0.65 T. To ensure saturation of the DG regardless of the field angle, the measurements have been repeated using a second setup, able to reach fields up to 9T, to extract the appropriate AMR and SMR values. The current applied through the Hall bridges was typically 100 μA .

The R_{SMR} and R_{AMR} constants of the previous equation are measured from $R_{xx}(\theta)$ measurements for an external magnetic field which is large enough to saturate the magnetization, rotating in the (xz) or (yz) plane, θ being the angle of the field with the film normal. To limit the Lorentz magnetoresistance, the magnetic field used for the measurement was slightly above the saturation field for each sample. For the DG, we find a negative contribution for the AMR and SMR effects: $R_{\text{AMR}}^{\text{DG}} = -18 \text{ m}\Omega$ and $R_{\text{SMR}}^{\text{DG}} = -108 \text{ m}\Omega$.

Micromagnetic simulations and 3D representation The simulations have been run using the micromagnetic solver *Mumax3* [27] and the following micromagnetic parameters: the exchange constant $A = 18$ pJ/m, the saturation magnetization $M_S = 1.2$ MA/m, the uniaxial surfacial anisotropy constant $K_{u,s} = 1.62$ mJ/m² and the DMI surfacial constant $D_s = 2.34$ pJ/m. To appropriately represent the complex structure

of the samples, cells of $2 \times 2 \times 2.1 \text{ nm}^3$ were used for the SG and $2 \times 2 \times 1.8 \text{ nm}^3$ for DG for a total simulation space of respectively $512 \times 512 \times 37$ and $512 \times 512 \times 121$ cells. As the domain wall can be thin in the strong PMA layers, and thus the magnetization can rotate over relatively short lengths (maximum angle below 30°), the simulations have been checked by running more precise simulations with $1 \times 1 \text{ nm}^2$ instead of $2 \times 2 \text{ nm}^2$ which did not yield a significant change in the magnetization distribution. Given the variable thickness, each trilayer was divided in three layers, one magnetic and the other two empty and the magnetic parameters were diluted depending on the experimental thickness of the given magnetic layer. In practice, we define the dilution factor $f = X_i/L_z$ with L_z the vertical dimension of the cells. Then, the micromagnetic parameters are updated: for the exchange, the DMI and the saturation magnetization, the constants are simply multiplied by f and for the anisotropy we set $K_u = K_u \times f - \mu_0 M_S^2 (f - f^2) / 2$ [36] with $K_u = K_{u,s}/X_i$.

The MFM images have been simulated using a lift height of 30 nm, using the method implemented in Mumax3.

For the electronic transport measurement simulations, the magnetization was initialized in a given direction (usually along y and z) with 50% noise and we swept the field from positives values to negative values. For helping the nucleation, we run at $T = 500 \text{ K}$ for 2 ns using a Gilbert damping parameters $\alpha = 0.01$ at the positive fields. In the case of DG where the nucleation in the strong PMA layers could not always be achieved by solely playing with the temperature or the magnetic noise, the nucleation was artificially induced by implementing one or two small skyrmions (radius of 15 nm) in the strong PMA layers and letting relax at different fields chosen to be coherent with the R_{xy} measurements and the hysteresis measurements. The various components of the magnetization were then extracted and weighted if needed to compare with the transport measurements. Since the SMR is mostly an interfacial effect, the magnetization of each layer has not been normalized by its associated Co thickness, contrarily to the AHE and AMR which are more intertwined with the Co layer thickness.

In most of the simulations, Bloch lines are present due to the noisy initialization even though they are not energetically favorable. To reduce their number, the magnetization tensor was subsampled by a factor 4 and ran for 0.5 ns in Mumax3. Then, it was resized to its original size and finally relaxed to a stable state which was very similar to the original one, minus most of the Bloch lines.

The output of the micromagnetic simulations have been represented using the software *Voxler4* after taking out the vacuum layers and using a multiplicative factor in the vertical direction of 1.6 for the SG and 3.3 for the DG.

References

- [1] Albert Fert, Nicolas Reyren, and Vincent Cros. Magnetic skyrmions: advances in physics and potential applications. *Nature Reviews Materials*, 2(7):1–15, 2017.
- [2] Karin Everschor-Sitte, Jan Masell, Robert M Reeve, and Mathias Kläui. Perspective: Magnetic skyrmions—overview of recent progress in an active research field. *Journal of Applied Physics*, 124(24):240901, 2018.
- [3] Naoto Nagaosa and Yoshinori Tokura. Topological properties and dynamics of magnetic skyrmions. *Nature nanotechnology*, 8(12):899–911, 2013.
- [4] Sebastian Muhlbauer, Benedikt Binz, F Jonietz, Christian Pfleiderer, Achim Rosch, Anja Neubauer, Robert Georgii, and Peter Boni. Skyrmion lattice in a chiral magnet. *Science*, 323(5916):915–919, 2009.

- [5] William Legrand, Jean-Yves Chauleau, Davide Maccariello, Nicolas Reyren, Sophie Collin, Karim Bouze-houane, Nicolas Jaouen, Vincent Cros, and Albert Fert. Hybrid chiral domain walls and skyrmions in magnetic multilayers. *Science advances*, 4(7):eaat0415, 2018.
- [6] Börge Göbel, Ingrid Mertig, and Oleg A Tretiakov. Beyond skyrmions: Review and perspectives of alternative magnetic quasiparticles. *Physics Reports*, 895:1–28, 2021.
- [7] Amalio Fernández-Pacheco, Robert Streubel, Olivier Fruchart, Riccardo Hertel, Peter Fischer, and Russell P Cowburn. Three-dimensional nanomagnetism. *Nature communications*, 8(1):1–14, 2017.
- [8] M Redies, FR Lux, J-P Hanke, PM Buhl, GP Müller, NS Kiselev, S Blügel, and Y Mokrousov. Distinct magnetotransport and orbital fingerprints of chiral bobbbers. *Physical Review B*, 99(14):140407, 2019.
- [9] Fengshan Zheng, Filipp N Rybakov, Aleksandr B Borisov, Dongsheng Song, Shasha Wang, Zi-An Li, Haifeng Du, Nikolai S Kiselev, Jan Caron, András Kovács, et al. Experimental observation of chiral magnetic bobbbers in b20-type fege. *Nature Nanotechnology*, 13(6):451–455, 2018.
- [10] Gideon P Müller, Filipp N Rybakov, Hannes Jónsson, Stefan Blügel, and Nikolai S Kiselev. Coupled quasimonopoles in chiral magnets. *Physical Review B*, 101(18):184405, 2020.
- [11] Noah Kent, Neal Reynolds, David Raftrey, Ian TG Campbell, Selven Virasawmy, Scott Dhuey, Rajesh V Chopdekar, Aurelio Hierro-Rodriguez, Andrea Sorrentino, Eva Pereiro, et al. Creation and observation of hopfions in magnetic multilayer systems. *Nature communications*, 12(1):1–7, 2021.
- [12] Yizhou Liu, Roger K Lake, and Jiadong Zang. Binding a hopfion in a chiral magnet nanodisk. *Physical Review B*, 98(17):174437, 2018.
- [13] Paul Sutcliffe. Hopfions in chiral magnets. *Journal of Physics A: Mathematical and Theoretical*, 51(37):375401, 2018.
- [14] Filipp N Rybakov, Nikolai S Kiselev, Aleksandr B Borisov, Lukas Döring, Christof Melcher, and Stefan Blügel. Magnetic hopfions in solids. *arXiv preprint arXiv:1904.00250*, 2019.
- [15] Andrada-Oana Mandru, Oğuz Yıldırım, Riccardo Tomasello, Paul Heistracher, Marcos Penedo, Anna Giordano, Dieter Suess, Giovanni Finocchio, and Hans Josef Hug. Coexistence of distinct skyrmion phases observed in hybrid ferromagnetic/ferrimagnetic multilayers. *Nature communications*, 11(1):1–7, 2020.
- [16] Oguz Yildirim, Riccardo Tomasello, Yaoxuan Feng, Giovanni Carlotti, Silvia Tacchi, Pegah Mirzadeh Vaghefi, Anna Giordano, Tanmay Dutta, Giovanni Finocchio, Hans J Hug, et al. Tuning the coexistence regime of incomplete and tubular skyrmions in ferro/ferri/ferromagnetic trilayers. *arXiv preprint arXiv:2204.06808*, 2022.
- [17] Katharina Witte, Andreas Späth, Simone Finizio, Claire Donnelly, Benjamin Watts, Blagoj Sarafimov, Michal Odrsticil, Manuel Guizar-Sicairos, Mirko Holler, Rainer H Fink, et al. From 2d stxm to 3d imaging: soft x-ray laminography of thin specimens. *Nano Letters*, 20(2):1305–1314, 2020.
- [18] Claire Donnelly, Manuel Guizar-Sicairos, Valerio Scagnoli, Sebastian Gliga, Mirko Holler, Jörg Raabe, and Laura J Heyderman. Three-dimensional magnetization structures revealed with x-ray vector nanotomography. *Nature*, 547(7663):328–331, 2017.

- [19] Claire Donnelly, Konstantin L Metlov, Valerio Scagnoli, Manuel Guizar-Sicairos, Mirko Holler, Nicholas S Bingham, Jörg Raabe, Laura J Heyderman, Nigel R Cooper, and Sebastian Gliga. Experimental observation of vortex rings in a bulk magnet. *Nature Physics*, 17(3):316–321, 2021.
- [20] S Seki, M Suzuki, M Ishibashi, R Takagi, ND Khanh, Y Shiota, K Shibata, W Koshibae, Y Tokura, and T Ono. Direct visualization of the three-dimensional shape of skyrmion strings in a noncentrosymmetric magnet. *Nature materials*, 21(2):181–187, 2022.
- [21] Daniel Wolf, Sebastian Schneider, Ulrich K Röckler, András Kovács, Marcus Schmidt, Rafal E Dunin-Borkowski, Bernd Büchner, Bernd Rellinghaus, and Axel Lubk. Unveiling the three-dimensional magnetic texture of skyrmion tubes. *Nature nanotechnology*, pages 1–6, 2021.
- [22] William Legrand, Yanis Sassi, Fernando Ajejas, Sophie Collin, Laura Bocher, Hongying Jia, Markus Hoffmann, Bernd Zimmermann, Stefan Blügel, Nicolas Reyren, et al. Spatial extent of the dzyaloshinskii-moriya interaction at metallic interfaces. *Physical Review Materials*, 6(2):024408, 2022.
- [23] Fernando Ajejas, Yanis Sassi, William Legrand, Sophie Collin, André Thiaville, Jose Peña Garcia, Stefania Pizzini, Nicolas Reyren, Vincent Cros, and Albert Fert. Element-selective modulation of interfacial dzyaloshinskii-moriya interaction in pt| co| metal based multilayers. *arXiv preprint arXiv:2109.00761*, 2021.
- [24] Yong-Keun Park, Dae-Yun Kim, Joo-Sung Kim, Yune-Seok Nam, Min-Ho Park, Hyeok-Cheol Choi, Byoung-Chul Min, and Sug-Bong Choe. Experimental observation of the correlation between the interfacial dzyaloshinskii-moriya interaction and work function in metallic magnetic trilayers. *NPG Asia Materials*, 10(10):995–1001, 2018.
- [25] AN Bogdanov and UK Röckler. Chiral symmetry breaking in magnetic thin films and multilayers. *Physical review letters*, 87(3):037203, 2001.
- [26] Matthias Bode, M Heide, K Von Bergmann, P Ferriani, Stefan Heinze, G Bihlmayer, A Kubetzka, O Pietzsch, Stefan Blügel, and R Wiesendanger. Chiral magnetic order at surfaces driven by inversion asymmetry. *Nature*, 447(7141):190–193, 2007.
- [27] Arne Vansteenkiste, Jonathan Leliaert, Mykola Dvornik, Mathias Helsen, Felipe Garcia-Sanchez, and Bartel Van Waeyenberge. The design and verification of mumax3. *AIP advances*, 4(10):107133, 2014.
- [28] Davide Maccariello, William Legrand, Nicolas Reyren, Fernando Ajejas, Karim Bouzehouane, Sophie Collin, Jean-Marie George, Vincent Cros, and Albert Fert. Electrical signature of noncollinear magnetic textures in synthetic antiferromagnets. *Physical Review Applied*, 14(5):051001, 2020.
- [29] TH Dang, Q Barbedienne, DQ To, E Rongione, N Reyren, F Godel, S Collin, JM George, and H Jaffrès. Anomalous hall effect in 3 d/5 d multilayers mediated by interface scattering and nonlocal spin conductivity. *Physical Review B*, 102(14):144405, 2020.
- [30] Yan-Ting Chen, Saburo Takahashi, Hiroyasu Nakayama, Matthias Althammer, Sebastian TB Goennenwein, Eiji Saitoh, and Gerrit EW Bauer. Theory of spin hall magnetoresistance. *Physical Review B*, 87(14):144411, 2013.

- [31] A Kobs, S Heße, W Kreuzpaintner, G Winkler, D Lott, P Weinberger, A Schreyer, and HP Oepen. Anisotropic interface magnetoresistance in pt/co/pt sandwiches. *Physical review letters*, 106(21):217207, 2011.
- [32] T McGuire and RL Potter. Anisotropic magnetoresistance in ferromagnetic 3d alloys. *IEEE Transactions on Magnetism*, 11(4):1018–1038, 1975.
- [33] Naoto Nagaosa, Jairo Sinova, Shigeki Onoda, Allan H MacDonald, and Nai Phuan Ong. Anomalous hall effect. *Reviews of modern physics*, 82(2):1539, 2010.
- [34] Davide Maccariello, William Legrand, Nicolas Reyren, Karin Garcia, Karim Bouzehouane, Sophie Collin, Vincent Cros, and Albert Fert. Electrical detection of single magnetic skyrmions in metallic multilayers at room temperature. *Nature nanotechnology*, 13(3):233–237, 2018.
- [35] D Nečas and P Klapetek. Gwyddion-free spm (afm, snom/nsom, stm, mfm,...) data analysis software.
- [36] Ivan Lemes, Felix Büttner, and Geoffrey SD Beach. Accurate model of the stripe domain phase of perpendicularly magnetized multilayers. *Physical Review B*, 95(17):174423, 2017.